RESEARCH

Alteration in the Structural, Optical, Thermal, Electrical, and Dielectric Properties of PMMA/PVDF Blend by Incorporation of Ni/ZnO Nanohybrid for Optoelectronic and Energy Storage Devices

A. Rajeh[1] · Hanan A. Althobaiti[2] · Samar J. Almehmadi[3] · Hessa A. Alsalmah[4] · N. A. Masmali[5] · Ahlam I. Al-Sulami[6] · Maryam Al-Ejji[7]

Abstract

In order to produce suitable poly(methyl methacrylate)/poly(vinylidene fluoride) (PMMA/PVDF) films for optoelectronic and power storage uses, Ni-doped ZnO nanoparticles were added to PMMA/PVDF films. This was done in order to generate a synergistic interaction between the superior electrical characteristics of Ni and the remarkable optical characteristics of ZnO NPs. The production of Ni/ZnO in wurtzite hexagonal phase with a normal grain size of 19 nm was verified by the findings of the selected-area diffraction of electrons and X-ray diffraction techniques. By using FTIR measurements, the interaction of polymers with Ni/ZnO has been studied. The raising of the Ni/ZnO content steadily redshifted the optical band gap. With various nanoparticle concentrations, the differential scanning calorimetry (DSC) results revealed an enhancement in the temperature of melting of the PMMA/PVDF-Ni/ZnO nanocomposites films as well as decrease in the level of crystallinity. At room temperature, an AC impedance study was carried out to check the electrical conductivity. All samples' ac conductivity spectra confirmed Jonscher's power law (JPL) behavior. The PMMA/PVDF-1.5%Ni/ZnO nanocomposites were discovered to have a greater ionic conductivity (σ_{ac}) of $1.10\ 10^{-5}$ S/cm at ambient temperature. Research on dielectric permittivity has additionally been carried out in order to comprehend the charge storage characteristics. The findings of the experiments showed that these PMMA/PVDF-Ni/ZnO films would provide excellent options for thermal insulators, cutting-edge microelectronics, capacitive storage of energy, optoelectronic technology and other applications.

Keywords Ni/ZnO nanoparticles · Optical properties · DSC analysis · Dielectric parameters · Ac conductivity

1 Introduction

In electronic and power generation systems including automobile, green energy production, healthcare equipment, and conversion systems, It is very important to consider the electric power storage with dielectric material [1, 2]. Electric-field-induced polarization of dielectric materials, which is necessary for the storage of electrical energy, demands materials that have substantial dielectric permittivity and significant breakdown intensities. Biaxially focused

✉ A. Rajeh
   a.rajeh88@yahoo.com

✉ Hessa A. Alsalmah
   haALSALMAH@imamu.edu.sa

1 Physics Department, Faculty of Applied Science, Amran University, Sana'a, Yemen

2 Physics Department, Collage of Science, Taif University, P.O. Box 11099, Taif 21944, Saudi Arabia

3 Department of Chemistry, Faculty of Applied Science, Umm Al Qura University, Makkah 24230, Saudi Arabia

4 Department of Physics, College of Science, Imam Mohammad Ibn Saud Islamic University (IMSIU), Riyadh 11623, Saudi Arabia

5 Department of Physics, College of Science, Jazan University, Jazan, Saudi Arabia

6 Department of Chemistry, College of Science, , University of Jeddah, Jeddah, Saudi Arabia

7 Center for Advanced Materials, Qatar University, P. O Box 2713, Doha, Qatar

polypropylene (BOPP), which has an elevated breakdown power with little dielectric loss and which is simple to manufacture, is now used extensively as an electric power storage dielectric product. However, polypropylene has a low volumetric energy density (~2 J/cm^3) due to its relatively low permittivity (εr = 2.2), which limits its use in integrated systems or mobile electronics [3]. Thus, the creation of cutting-edge dielectric materials with superior storage of energy capability is crucial for the development of next-generation technologies for storage energy. One of the most potential materials for dielectrics for high-energy capacity, according to current research, is poly (vinylidene fluoride) (PVDF) and its copolymers. [4]. Significant work has been done for producing high-performance PVDF-based polymers using the combining of nanocomposites [5], blending [6], laminating [7], coating [8], spinning [9], and so on. When using inorganic nanofillers, the nanocomposites approach among them has the benefit of increasing the dielectric permittivity [10]. For instance, PVDF containing high- εr BaTiO3 nanoparticles might enhance permittivity by a number of times [11]. However, the polymer blending technique, such as the one which involves using the blending of polymethyl methacrylate (PMMA), has the potential to increase insulating qualities, particularly by increasing breakdown strength[[12]. Yet there hasn't been much research on utilizing loans and nanocomposite in PVDF systems for energy storage. Although numerous earlier studies have looked into manufacturing technology [13, 14], dielectric permittivity [15], electrochemical and thermal properties [16] for blending nanocomposite materials, it is still an interesting mystery how blending and nanocomposite materials can have a synergistic impact on the efficiency of energy storage. The Strong bonds of hydrogen between the carbonyl groups of PMMA and the CH$_2$ group of PVDF, as well as efficient dipole connections between the methyl CH$_2$ group of PMMA and the CF$_2$ group of PVDF, are what make these two polymers miscible [17]. It's important to note that when PVDF is blended with PMMA, it crystallizes in the β-phase and the manufacturing cost is also greatly reduced [18]. Based on review of the literature, investigations on PVDF/PMMA blends have looked at their optical, mechanical, electrical, and thermal behavior [19]. The polymer works as a carrier to promote transport while the polyvinyl alcohol is being modified with Melamine-Formaldehyde and NiO nanoparticles [20]. In contrary to the corresponding virgin or blended polymers, metal oxide nanofillers usually improve the electrical, mechanical, optical, and thermal stability of the resultant polymer nanocomposites. The variation in the dielectric constant between the polymer matrix and loaded functional components is absorbed by semiconductor metal oxides like ZnO. Due to decreased MWS (Maxwell-Wagner-Sillars polarization) interfacial contact, this property

lowers leakage current [21]. The bond length along the axis is 0.96% longer in comparison to the other three bonds in ZnO4 groups, which are formed by the tetrahedral link between zinc and oxygen [22]. In order to increase the amount of the β phase content in PVDF, ZnO works as a nucleating agent and shows intrinsic ferroelectric and piezoelectric properties [23]. The primary objective of the current study is to cast Ni-doped ZnO nanoparticle-filled PMMA/PVDF nanocomposites films. We couldn't find any publications that have looked at the piezoelectric properties of Ni-doped ZnO-filled polymer nanocomposites. The β-phase fraction, filler dispersion, filler alignment, alignment of the polymer dipole moment, interactions present between the chains of polymers and also at the polymer-filler interfaces, and lattice strain produced by the fillers are the main factors that affect a polymer nanocomposite's piezoelectricity [24, 25]. In this work, Ni/ZnO nanoparticles are dispersed in a PMMA/PVDF blend, and the prepared PMMA/PVDF-Ni/ZnO nanocomposites are examined for the investigation of their structural, thermal, and optical characteristics, as well as their broadband dielectric dispersion and electrical conduction behavior.

2 Experimental work

2.1 Materials

PVDF (Sigma–Aldrich) with an average molecular weight of ca. 1.8×105 g mol^{-1}. The PMMA has average molecular weight Mw ~ 3.5×105 g mol^{-1} (SKU 445,746, a product of Germany). PVDF, PMMA, and Ni/ZnO nanohybrid were all dissolved using N-N, dimethylformamide (DMF) (Sigma Aldrich), which has a purity of 99.5%.

3 Preparation of Ni/ZnO Hybrids

The following procedure was used to make Ni/ZnO hybrids [26]: 1 g of CTAB was dissolved in 30 ml of distilled water until it produced a clear solution, and 8.1 mg of Zn(NO$_3$)$_2$ was then added while being continuously stirred for an hour. After that, to the aforesaid solution, 0.3 gm of Ni acetate that had been dissolved in 20 ml distilled water was added, and the mixture was agitated for two hours. For 24 h, the solution was left. The precipitate that was produced was filtered, washed several times with distilled water, and then dried for eight hours at 80 $^\circ$C. The precipitate that was produced was then calcined at 500 $^\circ$C for two hours.

3.1 Preparation of Samples

The two types of polymer, PVDF and PMMA, were prepared using the casting technique. The two polymers were dissolved in DMF, separately, from each polymer, and then we mixed the solution to prepare PMMA/PVDF blend (80/20 wt%). The solution was stirred continuously at room temperature to create a homogeneous solution. After that, for 45 min, Ni/ZnO powder was dissolved and suspended in DMF using a stirrer and a sonicator. To establish a uniform distribution of Ni/ZnO NPs in the matrix, several concentrations of Ni/ZnO (0.3, 0.7, 1.0, and 1.5 wt%) were added to the composite mixture as a dopant and mixed and sonicated for an additional 20 min. The mixture was then poured onto a glass plate to create uniformly thick nanocomposites. The film was dried for 15 h at 60 oC in a vacuum oven. To achieve homogenous Ni/ZnO dispersion in the polymer matrix, the resulting films were finely sliced. Some chosen samples had thicknesses that ranged from 0.03 to 0.2 mm for examination.

3.2 Characterization

On a PANalytical X'Pert PROXRD analyzer, the X-ray pattern was captured using filtered CuKα radiation ($\lambda = 1.54056$ oA), 30 kV accelerating, 10 mA X-ray tube current, 0.05° min^{-1} scan steps, and a 1s acquisition period. In order to study their structure, FTIR spectra were taken in the wave number range of 500 to 4000 cm^{-1} using a Nicolet iS10, USA spectrometer with a resolution of 4 cm^{-1}. Using a Japanese spectrophotometer (V-570 UV/VIS/NIR, JASCO), the UV-visible (UV-vis) absorption spectra of polymer films were measured in the wavelength range of 195–900 nm. A V2 6D TA instrument model DSC 2010 was used to evaluate differential scanning calorimetry (DSC) investigations in an inert environment at a heating rate of 10 °C/min. Using a broadband dielectric (Novocontrol Turnkey, Concept 40 System) in the range of 10 Hz to 7 MHz at room temperature, the conductivity behavior of the nanocomposite samples was investigated.

## 4 Results and Discussion

4.1 XRD Examination

The XRD analysis was used to examine the structure of the Ni/ZnO NPs and polymer nanocomposites films. Figure 1a clearly shows the main peaks of the Ni/ZnO NPs XRD pattern at $2\theta = 31.85°$, $34.46°$, $36.52°$, $47.81°$, $56.74°$, $62.78°$, $66.72°$, $68°0.23$, $69.17°$ and $77.21°$. According to the standard card (JCPDS of 89–0510), the hexagonal Wurtzite ZnO structure was indexed [26]. No NiO diffraction pattern was seen, suggesting that NiO crystals were dispersed over the ZnO surface. The XRD analysis of pure PVDF/PMMA film and PVDF/PMMA incorporated with various content of Ni/ZnO is exhibited in Fig. 1b. The wide peaks at 2θ values between 10.62° to 23.62° were seen in the pure PVDF/PMMA blend's XRD pattern, which clarifies the polymer blend's multiphase semicrystalline structure [27, 28]. The electroactive polar-phase crystals are explored by the reported diffraction peaks at 20.62 and 27.6, with the possibility of α-phase crystals merging with the β-phase [27]. Because of the low crystallinity of PVDF in the composites, the diffractions of PVDF were hardly detected [29]. With a rise in Ni/ZnO NPs concentration, the relative intensity of this wide peak diminishes. It demonstrates how the host polymer mixture gets more amorphous as Ni/ZnO concentration rises. Hodge et al.'s interpretation of this finding [30] suggested a relationship between the peak's intensity and crystallinity level. They claimed that when the amount of dopant is added, the intensity of the XRD pattern diminishes as the amount of amorphous nature grows. Amorphous polymers with flexible backbones exhibit higher ionic conductivity and stronger ionic diffusivity as a result of their amorphous character [31]. Additionally, it can see the emergence of new peaks in the nanocomposites sample (1.5wt.%Ni/ZnO) at the angles 31.85°, 34.46°, 36.52°, 47.81°, 56.74°, 62.78°, and 66.72°of the Ni/ZnO nanohybrid. This shows the existence of the nanoparticles in the polymer nanocomposites and some interactions between the polymer chains and Ni/ZnO nanoparticles. For the PMMA/PVDF blend and nanocomposites films, the integrated area of the polymer diffraction peaks and the hump area in the XRD traces across the range of 10° to 25° were utilized to calculate the values of percent crystallinity Xc (%) [32]. In Table 1, the observed Xc values for various nanocomposites are listed. It was encountered that the addition of the Ni/ZnO nanoparticles decreased the Xc values of the PMMA/PVDF blend via about 20% and after that, the reduction was noted as relatively small at 1.5wt% Ni/ZnO. When only a tiny number of Ni/ZnO nanoparticles were originally dispersed in the PMMA/PVDF mix, there is evidence of considerable modification in the structural blend due to the nanoparticles' electrostatic interaction with the blend.

4.2 UV-Vis Analysis

Figure 2 displays the optical absorption spectra of Ni/ZnO NPs doped PMMA/PVDF films and pure PMMA/PVDF films acquired at RT using a UV-Vis spectrometer. By using the absorption edge to calculate the band gaps of the films, one may learn important information about the band structure in both crystalline and non-crystalline states. The basic

Fig. 1 XRD patterns of (**a**) pure Ni/ZnO and (**b**) pure blend and nanocomposites films
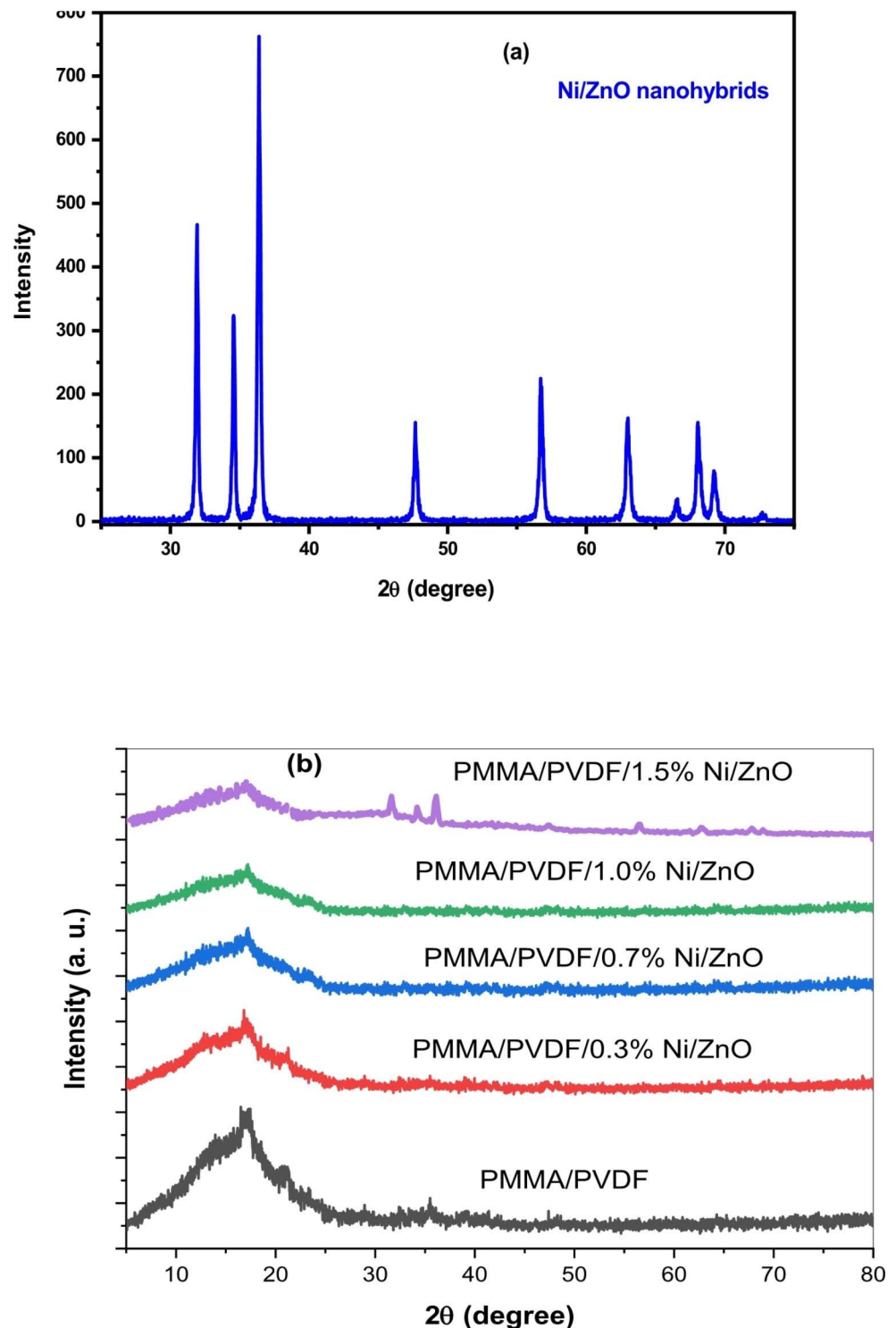
absorption principle is that electrons are stimulated from the valence band to the conduction band. The electronic transition from the bonding molecular orbit may be responsible for the small increase in absorbance seen for all doped samples when compared to pure film (Fig. 2). Peaks in the spectra may be seen at 215 and 250 nm. This band can be attributed to electronic transitions from the carbonyl $(C=O)$ groups of monomers in the PMMA chain as well as the $(-CF_2)$ groups in the repeat unit of the PVDF chain [33]. Additionally, the charge transfer (CT) bands typically seen for noncrystalline materials may be attributed to these optical absorption bands in the UV range. It is noticed that the increased absorbance for UV radiations is practically equal to that of the films made from PMMA/PVDF-Ni/ZnO nanocomposites
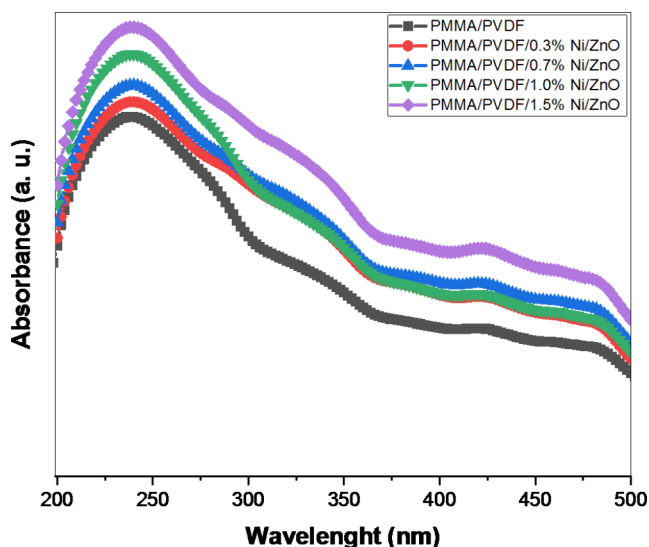
Fig. 2 UV–visible absorption spectra pure blend and nanocomposites films

loaded with wide band gap Ni/ZnO nanoparticles [34]. As previously shown, the PMMA/PVDF-Ni/ZnO nanocomposites films' distinctive behavior validated its usefulness as UV shielders in the development of next-generation optical systems [34]. Additionally, Fig. 2 shows that when the Ni/ZnO content in the PMMA/PVDF-Ni/ZnO nanocomposites films increased, the UV absorbance band displayed little red shift. An understanding of the establishment of inters-/intramolecular hydrogen bonds between Ni/ZnO ions and the neighboring functional groups of the PMMA/PVDF matrix are provided by the shift in the absorption band. According to Beer's law, the rising Ni/ZnO concentration will tend to enhance UV absorbance as well as intra- and interhydrogen bonding. According to presumptive explanations, the observed shift in the absorption edge of the different Ni/ZnO-doped PMMA/PVDF composite films is caused by the phase change (from crystalline to amorphous phase) that occurs after Ni/ZnO loading, which may eventually be reflected in the energy band gap [35]. There was no discernible peak in the absorption spectra of polymeric nanocomposites. This demonstrated that the synthetic specimen may be used as a UV-shielding block, UV filter, or UV reflector, which would be most suited for application in plastics, coatings, fibers, and cosmetics.

The Tauc equation was used to compute the optical energy gap values (Eg) of the pure PMMA/PVDF and
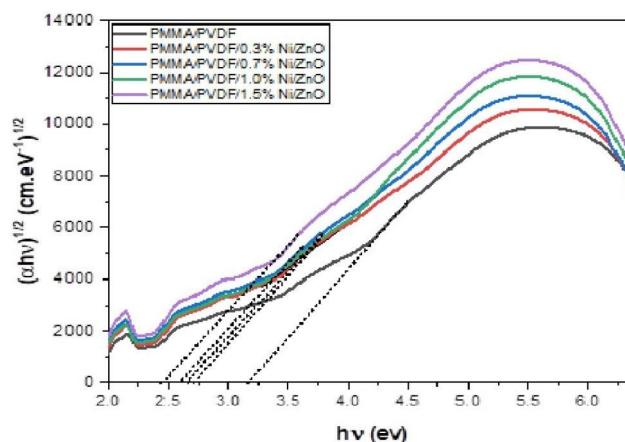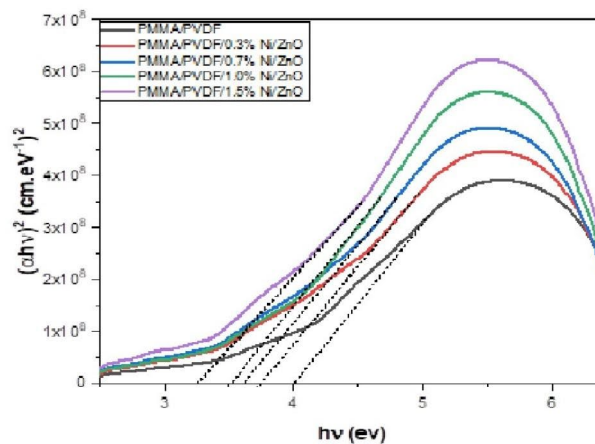
Fig. 3 Variation of (**a**) $(\alpha h\upsilon)^2$ and (**b**) $(\alpha h\upsilon)^{1/2}$ versus $h\upsilon$ of the prepared films

PMMA/PVDF-Ni/ZnO nanocomposites thin films from the high absorption area near the high absorption edge of these films [36]:

$$(\alpha h\nu) = B(h\nu - Eg)^r \qquad (3)$$

This equation is used to calculate the optical energy gap (Eg) values by plotting the relations $(\alpha h\upsilon)^2$ and $(\alpha h\upsilon)^{1/2}$ versus photon energy ($h\upsilon$). Figure 3(a, b), shows the variation of $(\alpha h\upsilon)^2$ and $(\alpha h\upsilon)^{1/2}$ as a function of ($h\nu$) for PMMA/PVDF-Ni/ZnO nanocomposites' thin films. It is notable that PMMA/PVDF has an optical energy gap value of 4.98 eV. Table 1 shows the optical energy gap for PMMA/PVDF after adding 0.3, 0.7, 1.0, and 1.5 wt% of Ni/ZnONPs. The

Table 1 The values for E_g^d, E_g^{ind}, and χc for the present films

Samples	Eg^d (eV)	Eg^{in} (eV)	Degree of crystallinity (X_c)
Pure PMMA/PVDF	4.00	3.16	23.45
PMMA/PVDF − 0.3% Ni/ZnONPs	3.73	2.73	22.15
PMMA/PVDF-0.7% Ni/ZnO NPs	3.62	2.62	20.95
PMMA/PVDF − 1.0%Ni/ZnO NPs	3.49	2.58	19.05
PMMA/PVDF-1.5% Ni/ZnO NPs	3.25	2.44	18.16

Fig. 4 The DSC thermograms of the prepared films
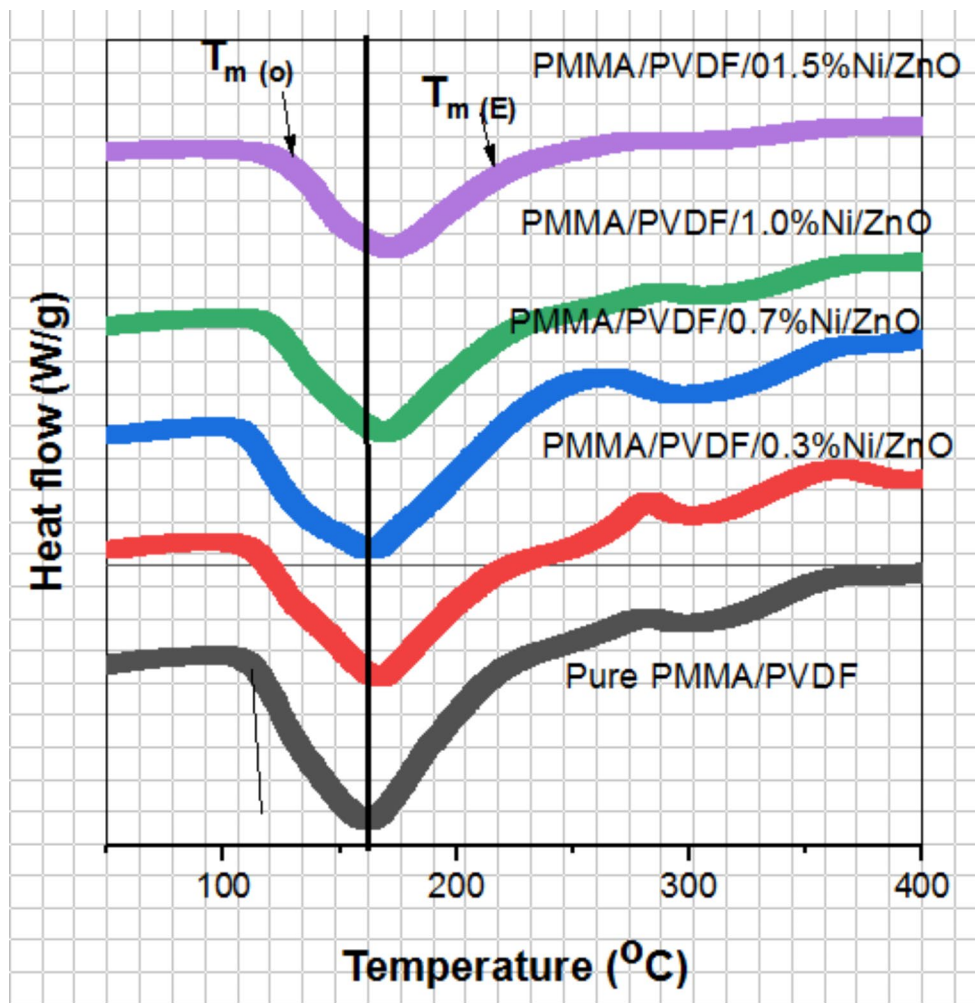
Table 2 Values of $T_{m(P)}$, $T_{m(O)}$, $T_{m(E)}$, ΔT_m, ΔH_m, and Xc determined from DSC thermograms for the blend/Ni/ZnO films

Samples	$T_{m(P)}$ (°C)	$T_{m(O)}$ (°C)	$T_{m(E)}$ (°C)	ΔT_m (°C)	ΔH_m (J/g)	Xc
PMMA/PVDF	160.32	113.45	210.34	96.89	22.56	21.52
PMMA/PVDF-0.3%Ni/ZnO	167.45	116.34	212.27	95.93	21.22	20.24
PMMA/PVDF- 0.7%Ni/ZnO	168.43	119.21	215.23	96.02	19.92	19.10
PMMA/PVDF-1.0% Ni/ZnO	169.58	122.45	217.21	94.76	18.52	17.67
PMMA/PVDF- 1.5%Ni/ZnO	172.87	128.12	223.79	95.67	18.02	17.19

optical energy gap of PMMA/PVDF is reduced from 4.00 to 3.25 eV (direct) and 3.16 to 2.44 eV (indirect) by changing the weight ratio of Ni/ZnO. Due to the interaction between Ni/ZnONPs and polymer matrix, unstructured defects and micro-strains were produced, which are what is responsible for the decrease in E_g values of PMMA/PVDF [37]. The density of localized states in the band gap rises as unstructured defects and micro-strains are produced [38].

4.3 Thermal Studies of PNC Films

The DSC thermograms of pure PMMA/PVDF and Ni/ZnO NPs doped PMMA/PVDF films from 50 to 400 °C are shown in Fig. 4. The melting temperature of PMMA/PVDF corresponded to the sole endothermic peak that was found. From the endothermic peaks for these films, the melting peak enthalpies of the PVDF crystallites were calculated and documented in Table 2. Recent literature provides a detailed explanation of the importance of these melting temperatures in relation to the thermal behavior of the crystalline phases [34, 39]. According to Fig. 4, when the concentration of Ni/ZnO nanofiller was raised from 0 to 1.5 wt%, the Tm values of these nanocomposites films altered abnormally in the region of 160–175 C. This fluctuation in Tm values showed that the inclusion of Ni/ZnO nanoparticles greatly alters the morphology of the mixed host matrix [33]. Additionally,

as Ni/ZnO NP doping is increased, the melting temperature of the PMMA/PVDF mix rises somewhat (from 160 to 175 °C), which is caused by the disturbance of the rotation and mobility of the polymer chain. The melting point rises as the energy barrier thickens [40]. Additionally, films made of nanocomposites with higher Tm values are more thermally stable [41]. The PMMA/PVDF-Ni/ZnO films' high Tm value suggested that they could have been used as thermal insulators in cutting-edge flexible electronics. These nanocomposites films' PVDF degree of crystallinity (Xc%) was calculated using a melting enthalpy(ΔH_m)-related relationship $Xc\% = (\Delta H_f/\Delta H_m) \times 100$, where the melting enthalpy of 100% crystalline PVDF material is $\Delta Hm = 104.8$ J/g, as shown in some earlier work [39, 42]. After adding Ni/ZnO NPs to the blend, the degree of PMMA/PVDF crystallinity values is shown in Table 2. It is obvious that the values of crystallinity degree alter erratically, although they remain higher than the value of the pure blend. Additionally, it was demonstrated that the PVDF crystalline Xc% values in these nanocomposites films, which were calculated from the XRD spectra and the DSC thermograms, are virtually similar with rising nanofiller concentration.

4.4 AC Conductivity Study

The variation of log σ_{ac} vs. log f for the prepared films at RT is seen in Fig. 5. There are two regions of this plot. The dispersion zone is in the lower frequency range. Because ions have time to build up on the electrode surface, the conductivity is frequently poor at these frequencies [43]. The higher frequency zone appears flat, showing that conductivity is not much affected by increasing frequency. The distance between localized states within the mixture was also impacted by the quantity of Ni/ZnO NPs, which in turn had an impact on the potential barriers separating them. As a
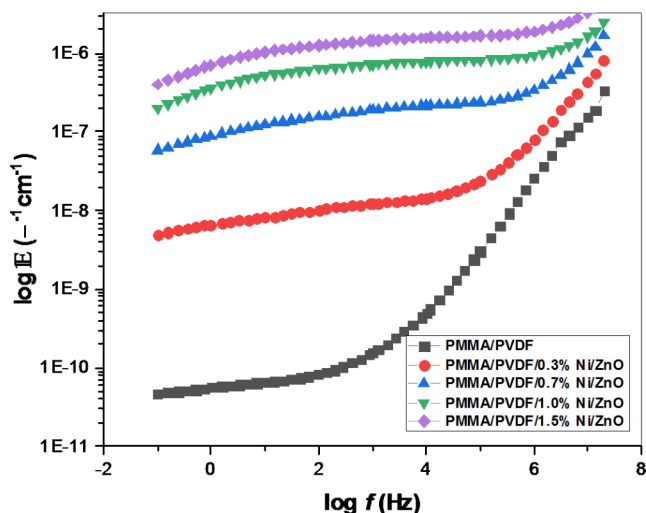
result, the mobility of the charges varied. Additionally, additional doping of Ni/ZnO NPs raised the blend's amorphous level; as a result, the free volume around the blended network rose, increasing the mobility of polarons and bipolrons [44]. Additionally, chain scissoring and further degradation of the polymer chains cause the electrical conductivity to rise the most following the addition of Ni/ZnO NPs, which speeds up ionic transport through the polymer model [45].

4.5 Dielectric Properties

The relationship between the dielectric constant (ϵ'), often known as the energy storage component, and the dielectric loss (ϵ''), is given by Eqs. (3 and 4) [46].

$$\epsilon' = Cd/\epsilon_o A \tag{3}$$

$$\epsilon'' = \sigma ac/\omega \epsilon_o \tag{4}$$

C describes capacitance, d is the material's thickness, ϵ_o is permittivity of free space's, and A is electrode's area. Figure 6 shows the dielectric constant (ϵ') and frequency-dependent dielectric loss (ϵ'') spectra for blended polymer films made of PMMA/PVDF and PMMA/PVDF/xwt% Ni/ZnO at RT. Since the permittivity/conductivity values for the host PMMA/PVDF mix and the Ni/ZnO have changed, the interfacial polarization (IP) "Maxwell-Wagner-Sillars (MWS) mechanism", which is present in the hybrid inorganic-organic structures, has changed as well, showed a maximum value of the ε′ and ε″ at a lower frequency, which was attributed to its significant participation [40, 41]. For all blend and blend/Ni/ZnO films, the values of ε′ and ε″ fell as frequency rose. The value of ε′ and ε″ decreases at higher frequencies because dipoles are unable to spin in the direction of the applied field. Additionally, the dipolar ordering of polar PMMA/PVDF was impacted by the electrostatic interactions of Ni/ZnO with dipolar groups, changing the doped blend's dielectric permittivity values [47]. Due to the characteristics of composite materials, which depend on the nature, concentration, and quantity of defects as well as the interfacial interaction between filler and polymer, nanofiller when added to PMMA/PVDF enhances the ε′ and ε″ in comparison to pristine PMMA/PVDF [48]. Through the accumulation of free ions, adding Ni/ZnO to PMMA/PVDF matrix produces micro-capacitance over the whole spectrum of the PMMA/PVDF blend. According to the MWS interface and space polarization hypothesis, this phenomenon results from a difference in electrical conductivity between crystal surfaces and amorphous regions [49]. Ni/ZnO loading thereby increases ε′ and ε″ at lower frequency ranges (10 Hz-7 MHz).

Fig. 5 Log σ_{ac} versus log f for the prepared films at RT.
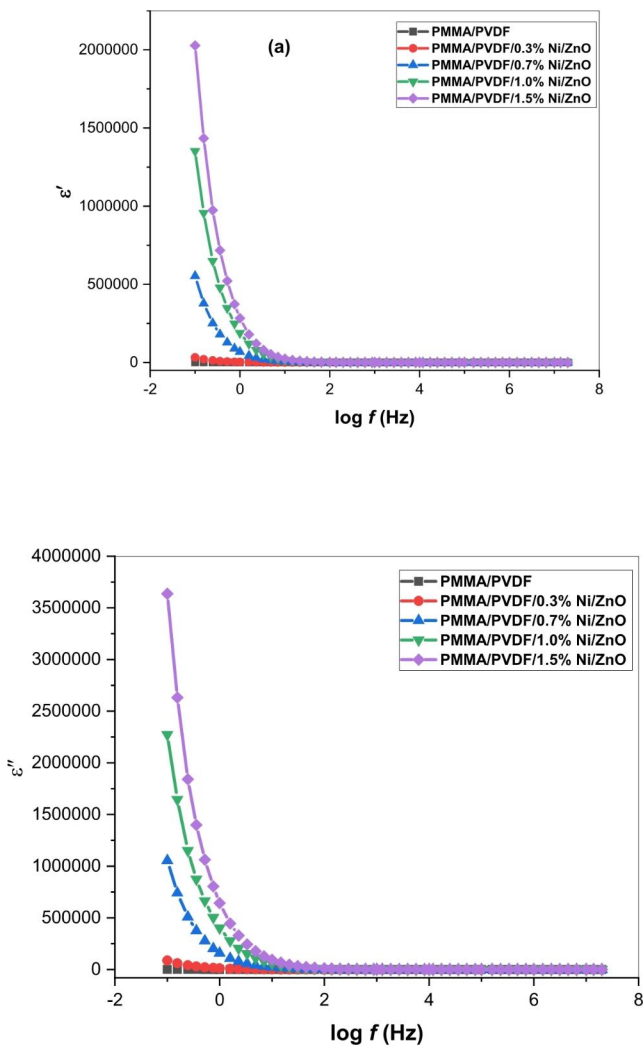
Fig. 6 Variation of the (**a**) ε′ and (**b**) ε″ versus log f for the prepared films at RT.
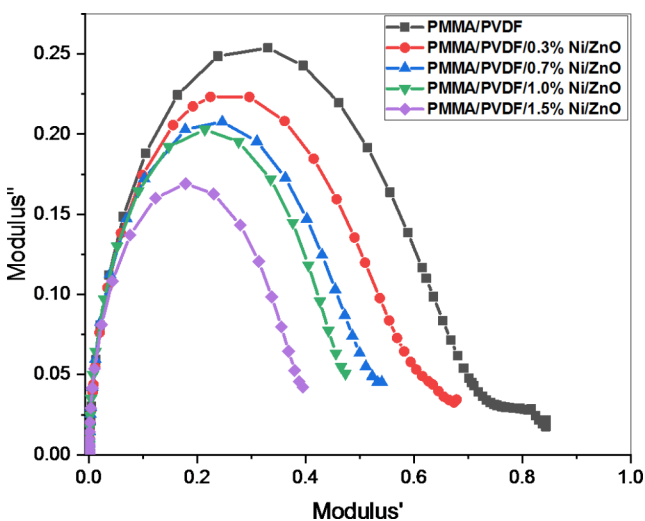
Fig. 7 Variation of the M′ and M″ for the prepared films at RT.

Additionally, the relaxation process in polymer nanocomposites is caused by ion conductivity and is depicted by an Argand plot. Figure 7 depicts the Argand plot for PMMA/PVDF and PMMA/PVDF/xwt% Ni/ZnO films, which is drawn between M′ and M″ at RT. This image's observed incomplete semicircle curves show non-Debye nature. The non-Debye behavior is caused by a variety of polarizations, the relaxation process, and many interactions between the ions and the dipoles [50]. The conductivity of the prepared films is well known to have a strong relationship with the arc radius [51]. The length of the arc is reduced when the Ni/ZnO ratio is raised, boosting conductivity as a result [52]. A single relaxation time may be calculated when the arc diameter of the M′ and M″ curves coincides with the M′ axis, indicating that the curves display a full semicircular arc. This is important for distinguishing between conductivity relaxation and viscoelastic relaxation processes. This implies that the Debye model and conductivity relaxation are compatible [53].

5 Conclusion

Solution casting was used to produce the polymer nanocomposites made of PMMA/PVDF and different Ni/ZnO NP concentrations. The produced nanocomposites samples exhibit amorphousness according to XRD examination, which also demonstrates the interaction of nanoparticles with the polymer matrix via a decline in crystallinity. The interaction between the nanoparticles and the polymer mixture was verified by the FT-IR. To determine if the films might be used in optoelectronics, their optical characteristics were examined. As the filler content grew from 0 to 1.5wt%, the direct bandgap reduced from 4.00 to 3.25 eV and the indirect band gap declined from 3.16 to 2.44 eV. The examination of thermal characteristics derived from DSC clearly indicated that the nanoparticles concentration in the PMMA/PVDF matrix greatly boosted the thermal stability of the nanocomposites samples. The PMMA/PVDF-Ni/ZnO films high melting point illustrates why they are used as flexible thermal insulators. The loading of nanoparticles was observed to improve the AC conductivity, and dielectric parameters loss of PMMA/PVDF-Ni/ZnO nanocomposites. The composite containing 1.5wt% of the sample demonstrated greater optical, AC conductivity and dielectric parameters characteristics in comparison to other samples. The energy gaps in the band that showed up in accordance with the electronic transition from the host PMMA/PVDF blend's functional groups and the distinctive transitions of the Ni/ZnO NPs material demonstrated the appropriateness of these flexible materials for the fabrication of

next-generation optoelectronic devices, thermal insulators, microelectronic, and devices for storing energy.

Author Contributions A. Rajeh: Supervision, Conceptualization, Formal analysis, Methodology, Writing – original draft, Writing – review & editing. Hanan A. Althobaiti: Writing – review, Visualization, Investigation, Software. Samar J. Almehmadi: Writing – review & editing Hessa A. Alsalmah: Data curation, Writing – review & editing, Visualization. N. A. Masmali: Visualization, Investigation, Data curation. Ahlam I. Al-Sulami: Writing – review & editing, Visualization, Data curation. Maryam Al-Ejji: Data curation, Writing – review & editing.

Declarations

Competing Interests The authors declare that they have no known competing financial interests or personal relationships that could have appeared to influence the work reported in this paper.

References

1. Q. Chen, Y. Shen, S. Zhang, Q.M. Zhang, Polymer-based dielectrics with High Energy Storage Density. Annu. Rev. Mater. Res. **45**, 433–458 (2015). https://doi.org/10.1146/annurev-matsci-070214-021017

2. M. Shahinpoor, K.J. Kim, D.J. Leo, Ionic polymer-metal composites as multifunctional materials. Polym. Compos. **24**, 24–33 (2003). https://doi.org/10.1002/pc.10002

3. B. Fan, M. Zhou, C. Zhang, D. He, J. Bai, Polymer-based materials for achieving high energy density film capacitors. Prog Polym. Sci. **97**, 101143 (2019). https://doi.org/10.1016/J.PROGPOLYMSCI.2019.06.003

4. B. Xie, Q. Zhang, L. Zhang, Y. Zhu, X. Guo, P. Fan, H. Zhang, Ultrahigh discharged energy density in polymer nanocomposites by designing linear/ferroelectric bilayer heterostructure. Nano Energy. **54**, 437–446 (2018). https://doi.org/10.1016/J.NANOEN.2018.10.041

5. C. Basavaraja, J.H. Jang, G.H. Jung, D.S. Huh, Magnetic and electrical properties of polypyrrole nanocomposites with iron nanoparticles attached to 2-acrylamido-2-methyl-1-propane-sulfonic acid. Polym. Compos. **35**, 364–371 (2014). https://doi.org/10.1002/pc.22669

6. M.A. Morsi, A. Rajeh, A.A. Al-Muntaser, Reinforcement of the optical, thermal and electrical properties of PEO based on MWCNTs/Au hybrid fillers: nanodielectric materials for organo-electronic devices. Compos. Part B: Eng. **173**, 106957 (2019)

7. J. Chen, Y. Wang, X. Xu, Q. Yuan, Y. Niu, Q. Wang, H. Wang, Sandwich structured poly(vinylidene fluoride)/polyacrylate elastomers with significantly enhanced electric displacement and energy density. J. Mater. Chem. A **6**, 24367–24377 (2018). https://doi.org/10.1039/C8TA09111K

8. M.M. Abutalib, A. Rajeh, Enhanced structural, electrical, mechanical properties and antibacterial activity of Cs/PEO doped mixed nanoparticles (Ag/TiO2) for food packaging applications. Polym. Test. **93**, 107013 (2021)

9. H. Liu, Y. Shen, Y. Song, C.-W. Nan, Y. Lin, X. Yang, Carbon Nanotube Array/Polymer Core/Shell Structured Composites with High Dielectric Permittivity, low dielectric loss, and large

10. energy density. Adv. Mater. **23**, 5104–5108 (2011). https://doi.org/10.1002/adma.201102079

10. Z. Shen, J. Wang, Y. Lin, C. Nan, L. Chen, Y. Shen, High-throughput Phase-Field Design of High-Energy-Density Polymer Nanocomposites. Adv. Mater. **30**, 1704380 (2018). https://doi.org/10.1002/adma.201704380

11. J.-W. Zha, Z.-M. Dang, T. Yang, T. Zhou, H.-T. Song, S.-T. Li, Advanced dielectric properties of BaTiO$_3$/polyvinylidene-fluoride nanocomposites with sandwich multi-layer structure. IEEE Trans. Dielectr. Electr. Insul. **19**, 1312–1317 (2012). https://doi.org/10.1109/TDEI.2012.6260006

12. M.-S. Zheng, J.-W. Zha, Y. Yang, P. Han, C.-H. Hu, Y.-Q. Wen, Z.-M. Dang, Polyurethane induced high breakdown strength and high energy storage density in polyurethane/poly(vinylidene fluoride) composite films. Appl. Phys. Lett. **110** (2017). https://doi.org/10.1063/1.4989579

13. T. Hosoda, T. Yamada, Morphological study of PVDF/PMMA/TiO2 blend films prepared by melt casting process. J. Polym. Eng. **33**, 639–649 (2013). https://doi.org/10.1515/polyeng-2013-0049

14. L. Liu, H. Chen, F. Yang, Enhancing membrane performance by blending ATRP grafted PMMA–TiO2 or PMMA–PSBMA–TiO2 in PVDF. Sep. Purif. Technol. **133**, 22–31 (2014). https://doi.org/10.1016/J.SEPPUR.2014.06.015

15. H. Alghamdi, Mohammed, A. Rajeh, Synthesis of CoFe2O4/MWCNTs nanohybrid and its effect on the optical, thermal, and conductivity of PVA/CMC composite as an application in electrochemical devices. J. Inorg. Organomet. Polym Mater. **32**(5), 1935–1949 (2022)

16. D. Song, C. Xu, Y. Chen, J. He, Y. Zhao, P. Li, W. Lin, F. Fu, Enhanced thermal and electrochemical properties of PVDF-HFP/PMMA polymer electrolyte by TiO2 nanoparticles. Solid State Ionics. **282**, 31–36 (2015). https://doi.org/10.1016/J.SSI.2015.09.017

17. $_3$ nanocomposites for optoelectronic and nanodielectric applications. J. Mater. Res.Tech. 26 (2023) 2310–2318

18. S.M. Pawde, K. Deshmukh, Investigation of the structural, thermal, mechanical, and optical properties of poly(methyl methacrylate) and poly(vinylidene fluoride) blends. J. Appl. Polym. Sci. **114**, 2169–2179 (2009). https://doi.org/10.1002/app.30641

19. C. Lei, X. Wang, D. Tu, H. Wang, Q. Du, Charge distribution in PVDF/PMMA blends under DC field. Mater. Chem. Phys. **114**, 272–278 (2009)

20. J. Choma, K. Jedynak, M. Marszewski, M. Jaroniec, Polymer-templated mesoporous carbons synthesized in the presence of nickel nanoparticles, nickel oxide nanoparticles, and nickel nitrate. Appl. Surf. Sci. **258**, 3763–3770 (2012)

21. L. Guan, L. Weng, X. Zhang, Z. Wu, Q. Li, L. Liu, Micro-structures, electrical behavior and energy storage properties of Ag@shell/PVDF-based polymers: different effects between an organic polydopamine shell and inorganic zinc oxide shell. J. Mater. Sci. **55**, 15238–15251 (2020). https://doi.org/10.1007/s10853-020-05081-9

22. Furhan, M.T. Ramesan, Development of conductive poly (para-aminophenol)/zinc oxide nanocomposites for optoelectronic devices. Polym. Bull. **80**(6), 6405–6432 (2023)

23. A.M. Chandran, S. Varun, S.C. Karumuthil, S. Varghese, P.K.S. Mural, Zinc oxide nanoparticles coated with (3-Aminopropyl) triethoxysilane as additives for boosting the Dielectric, Ferroelectric, and Piezoelectric Properties of Poly(vinylidene fluoride) Films for Energy Harvesting, ACS Appl. Nano Mater. **4**, 1798–1809 (2021). https://doi.org/10.1021/acsanm.0c03214

24. H. Wang, C. Zhang, B. Zhou, Z. Zhang, J. Shen, A. Du, Ultra-black carbon@silica core-shell aerogels with controllable electrical conductivities. Adv. Compos. Hybrid. Mater. **2**, 743–752 (2019). https://doi.org/10.1007/s42114-019-00123-6

25. M.A. Omri, A. Triki, M. Ben Hassen, M.R. Sanjay, M. Arous, A. Kallel, Effect of Alfa fiber mechanical separation on dielectric properties of hybrid unsaturated polyester composites. Polym. Compos. **40**, 1774–1785 (2019). https://doi.org/10.1002/pc.24934

26. H. Parangusan, D. Ponnamma, M. Al Ali, AlMaadeed, Flexible tri-layer piezoelectric nanogenerator based on PVDF-HFP/Ni-doped ZnO nanocomposites. RSC Adv. **7**, 50156–50165 (2017). https://doi.org/10.1039/C7RA10223B

27. F. Khan, T. Kowalchik, S. Roundy, R. Warren, Stretching-induced phase transitions in barium titanate-poly(vinylidene fluoride) flexible composite piezoelectric films. Scr. Mater. **193**, 64–70 (2021). https://doi.org/10.1016/J.SCRIPTAMAT.2020.10.036

28. L. Wan, W. Tian, N. Li, D. Chen, Q. Xu, H. Li, J. He, J. Lu, Hydrophilic porous PVDF membrane embedded with BaTiO3 featuring controlled oxygen vacancies for piezocatalytic water cleaning. Nano Energy. **94**, 106930 (2022). https://doi.org/10.1016/J.NANOEN.2022.106930

29. K. Behera, J.-F. Chen, J.-M. Yang, Y.-H. Chang, F.-C. Chiu, Evident improvement in burning anti-dripping performance, ductility and electrical conductivity of PLA/PVDF/PMMA ternary blend-based nanocomposites with additions of carbon nanotubes and organoclay. Compos. Part. B Eng. **248**, 110371 (2023). https://doi.org/10.1016/J.COMPOSITESB.2022.110371

30. R.M. Hodge, G.H. Edward, G.P. Simon, Water absorption and states of water in semicrystalline poly(vinyl alcohol) films. Polymer. **37**, 1371–1376 (1996). https://doi.org/10.1016/0032-3861(96)81134-7

31. M.M. Abutalib, A. Rajeh, Influence of ZnO/Ag nanoparticles doping on the structural, thermal, optical and electrical properties of PAM/PEO composite. Phys. B: Condens. Matter. **578**, 411796 (2020)

32. A. Rajeh, H.M. Ragab, M.M. Abutalib, Co doped ZnO reinforced PEMA/PMMA composite: structural, thermal, dielectric and electrical properties for electrochemical applications. J. Mol. Struct. **1217**, 128447 (2020)

33. R.J. Sengwa, N. Kumar, M. Saraswat, Morphological, structural, optical, broadband frequency range dielectric and electrical properties of PVDF/PMMA/BaTiO3 nanocomposites for futuristic microelectronic and optoelectronic technologies. Mater. Today Commun. **35**, 105625 (2023). https://doi.org/10.1016/J.MTCOMM.2023.105625

34. S. Suvarna, M.T. Ramesan, Optical and electrical properties of copper alumina nanoparticles reinforced chlorinated polyethylene composites for optoelectronic devices. J. Indian Chem. Soc. **99**(11), 100772 (2022)

35. K. Meera, M.T. Ramesan, Development of high-performance biopolymer nanocomposites derived from carboxymethyl chitosan/boehmite via green synthesis. Polym. Compos. **44**, 1135–1148 (2023). https://doi.org/10.1002/pc.27159

36. E.M. Abdelrazek et al., Modifying of structural, optical, thermal, and mechanical properties of PCL/PMMA biomaterial blend doped with MWCNTs as an application in materials science. J. Inorg. Organomet. Polym Mater. (2023) 1–10

37. K. Parvathi, Effect of titanium dioxide on the structural, thermal, and electrical properties of chlorinated natural rubber/poly (indole) blend nanocomposites for flexible nanoelectronic devices. J. Appl. Polym. Sci. **140**(11), e53621 (2023)

38. S. Pervaiz, N. Kanwal, S.A. Hussain, M. Saleem, I.A. Khan, Study of structural, optical and dielectric properties of ZnO/PVDF-based flexible sheets. J. Polym. Res. **28**, 309 (2021). https://doi.org/10.1007/s10965-021-02640-9

39. R.J. Sengwa, P. Dhatarwal, Toward multifunctionality of PEO/PMMA/MMT hybrid polymer nanocomposites: promising morphological, nanostructural, thermal, broadband dielectric, and optical properties. J. Phys. Chem. Solids. **166**, 110708 (2022). https://doi.org/10.1016/J.JPCS.2022.110708

40. Q.A. Alsulami, A. Rajeh, Synthesis of the SWCNTs/TiO2 nanostructure and its effect study on the thermal, optical, and conductivity properties of the CMC/PEO blend. Results Phys. **28**, 104675 (2021). https://doi.org/10.1016/J.RINP.2021.104675

41. Q.A. Alsulami, A. Rajeh, Structural, thermal, optical characterizations of polyaniline/polymethyl methacrylate composite doped by titanium dioxide nanoparticles as an application in optoelectronic devices. Opt. Mater. **123**, 111820 (2022)

42. S. Suvarna, Furhan, M.T. Ramesan, Structural, conductivity, mechanical and wettability properties of copper alumina reinforced chlorinated polyethylene/polyvinyl chloride blend nanocomposites. Res. Chem. Intermed. **49**(5), 1891–1908 (2023)

43. H.M. Alghamdi, A. Rajeh, Study of the photoluminescence, optical, thermal, and electrical parameters of the Cs/PVP blend/zinc oxide nanorods films for energy storage devices. Polym. Test. **124**, 108093 (2023)

44. K. Parvathi, M.T. Ramesan, Tailoring the structural, electrical and thermal properties of zinc oxide reinforced chlorinated natural rubber/poly (indole) blend nanocomposites for flexible electrochemical devices. J. Polym. Res. **30**(2), 55 (2023)

45. H. Alghamdi, Mohammed et al., Effect of the Fe_2O_3/TiO_2 nanoparticles on the structural, mechanical, electrical properties and antibacterial activity of the biodegradable chitosan/polyvinyl alcohol blend for food packaging. J. Polym. Environ. **30**(9), 3865–3874 (2022)

46. H. Albalawi, E.M. Alharbi, A.I. Al-Sulami, N. Al-Qahtani, M.O. Farea, A. Rajeh, Synthesis and characterization of sodium alginate/polyvinyl alcohol/zinc oxide/iron oxide nanocomposites for electrochemical applications. Polym. Compos. **44**, 1762–1771 (2023). https://doi.org/10.1002/pc.27203

47. Q.A. Alsulami, A. Rajeh, Modification and development in the microstructure of PVA/CMC-GO/Fe3O4 nanocomposites films as an application in energy storage devices and magnetic electronics industry. Ceram. Int. **49**, 14399–14407 (2023). https://doi.org/10.1016/J.CERAMINT.2023.01.029

48. M.R. Atta, N. Algethami, M.O. Farea, Q.A. Alsulami, A. Rajeh, Enhancing the structural, thermal, and dielectric properties of the polymer nanocomposites based on polymer blend and barium titanate nanoparticles for application in energy storage. Int. J. Energy Res. **46**, 8020–8029 (2022). https://doi.org/10.1002/er.7703

49. R. Magisetty, A. Shukla, B. Kandasubramanian, Dielectric, Hydrophobic investigation of ABS/NiFe2O4 nanocomposites fabricated by atomized spray assisted and Solution Casted Techniques for Miniaturized Electronic Applications. J. Electron. Mater. **47**, 5640–5656 (2018). https://doi.org/10.1007/s11664-018-6452-x

50. S. Sankar, M.T. Ramesan, Thermal, optical and temperature-dependent electrical properties of poly (aniline-co-pyrrole)/copper alumina nanocomposites for optoelectronic devices. J. Therm. Anal. Calorim. **147**(23), 13375–13387 (2022)

51. N. Algethami, Structural, optical, electrical, and DFT studies of chitosan/polyvinyl alcohol composite doped with mixed nanoparticles (GO/TiO2) for flexible energy-storage devices. J. Mater. Sci. Mater. Electron. **33**, 25518–25531 (2022). https://doi.org/10.1007/s10854-022-09252-z

52. H.M. Alghamdi, M.M. Abutalib, M.A. Mannaa, O. Nur, E.M. Abdelrazek, A. Rajeh, Modification and development of high bioactivities and environmentally safe polymer nanocomposites doped by Ni/ZnO nanohybrid for food packaging applications. J. Mater. Res. Technol. **19**, 3421–3432 (2022). https://doi.org/10.1016/J.JMRT.2022.06.077

53. H.S. Alzahrani, A.I. Al-Sulami, Q.A. Alsulami, A. Rajeh, A systematic study of structural, conductivity, linear, and nonlinear

optical properties of PEO/PVA-MWCNTs/ZnO nanocomposites films for optoelectronic applications. Opt. Mater. (Amst). **133**, 112900 (2022). https://doi.org/10.1016/J.OPTMAT.2022.112900

Publisher's Note Springer Nature remains neutral with regard to jurisdictional claims in published maps and institutional affiliations.